ACS APPLIED MATERIALS & INTERFACES

Research Article

Cite This: ACS Appl. Mater. Interfaces 2019, 11, 34305−34315

www.acsami.org

Miniaturized Flexible Piezoresistive Pressure Sensors: Poly(3,4-ethylenedioxythiophene):Poly(styrenesulfonate) Copolymers Blended with Graphene Oxide for Biomedical Applications

Jer-Chyi Wang,[*,†,‡,§,¶] Rajat Subhra Karmakar,[†] Yu-Jen Lu,[*,∥,¶] Shun-Hsiang Chan,[⊥] Ming-Chung Wu,[⊥,††] Kun-Ju Lin,[▽,○] Chin-Kuo Chen,[♦] Kuo-Chen Wei,[#,¶] and Yung-Hsin Hsu[‡‡]

[†]Department of Electronic Engineering, [‡]Biosensor Group, Biomedical Engineering Center, [∥]School of Traditional Chinese Medicine, [⊥]Department of Chemical and Materials Engineering, [#]School of Medicine, and [○]Department of Medical Imaging and Radiological Sciences, Chang Gung University, Guishan District, 33302 Taoyuan, Taiwan

[§]Department of Electronic Engineering, Ming Chi University of Technology, Taishan District, 24301 New Taipei City, Taiwan

[¶]Department of Neurosurgery, [▽]Department of Nuclear Medicine, [♦]Department of Otolaryngology, and [††]Division of Neonatology, Department of Pediatrics, Chang Gung Memorial Hospital, Linkou, Guishan District, 33305 Taoyuan, Taiwan

[‡‡]Department of Neurosurgery, Asia University Hospital, Wufeng District, 41354 Taichung, Taiwan

Supporting Information

ABSTRACT: Piezoresistive pressure sensors have garnered significant attention because of their wide applications in automobiles, intelligent buildings, and biomedicine. For in vivo testing, the size of pressure sensors is a vital factor to monitor the pressure of specific portions of a human body. Therefore, the primary focus of this study is to miniaturize piezoresistive pressure sensors with graphene oxide (GO)-incorporated poly(3,4-ethylenedioxythiophene):poly(styrenesulfonate) (PEDOT:PSS) composite films on a flexible substrate for biomedical applications. Prior to the fabrication of pressure sensors, a comprehensive material analysis was applied to identify the horizontal placement of GO flakes within the PEDOT:PSS copolymers, revealing a reduction in variable range hopping distance and an enhancement in carrier mobility. For devices scaled to 0.2 cm, the sensitivity of PEDOT:PSS pressure sensors was conspicuously decreased owing to the late response, which can be effectively solved by GO incorporation. Using technology computer-aided design simulations, the current crowded at the PEDOT:PSS film surface and in the vicinity of an indium−tin−oxide electrode corner was found to be responsible for the changes in piezoresistive behaviors of the scaled devices. The miniaturized flexible piezoresistive pressure sensors with PEDOT:PSS/GO composite films are capable of monitoring the brain pressure of intracranial surgery of a rat and discerning different styles of music for a potential application in hearing aids.

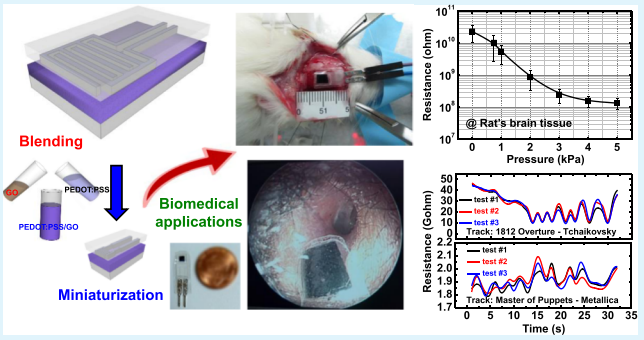

KEYWORDS: *poly(3,4-ethylenedioxythiophene):poly(styrenesulfonate) (PEDOT:PSS), piezoresistive, pressure sensor, graphene oxide, miniaturization, current crowding, flexible electronics, biomedicine*

INTRODUCTION

Flexible electronics are attractive emerging technologies which have been integrated in wearable devices.[1,2] Particularly, flexible pressure sensors have been used extensively for controlling and monitoring thousands of systems in biomedical, environmental, household, space, and automotive fields,[3−7] important for present industrial advancements. Three predominant pressure-sensing technologies exist in the market, that is, capacitive, piezoelectric, and piezoresistive pressure sensors.[8−10] Among them, piezoresistive pressure sensors are the most typically employed because of their high sensitivity and low cost.[10] The general materials used in piezoresistive pressure sensors are silicon-based thin films, bonded metal foils, conductive polymers, and so on.[11] For conductive polymers, particularly, poly(3,4-ethylenedioxythiophene):poly(styrenesulfonate) (PEDOT:PSS) is an excellent candidate for piezoresistive flexible electronics applications[12−15] because of its high electrochemical and thermal stability, high conductivity, favorable optical properties, and high transparency.[16,17] It is well known that PEDOT is a conductive polymer with 3,4-ethylenedioxythiophene (EDOT) monomer, and polystyrene sulfonic acid (PSS) is introduced to form

Received: June 20, 2019
Accepted: August 27, 2019
Published: August 27, 2019

DOI: 10.1021/acsami.9b10575
ACS Appl. Mater. Interfaces 2019, 11, 34305−34315

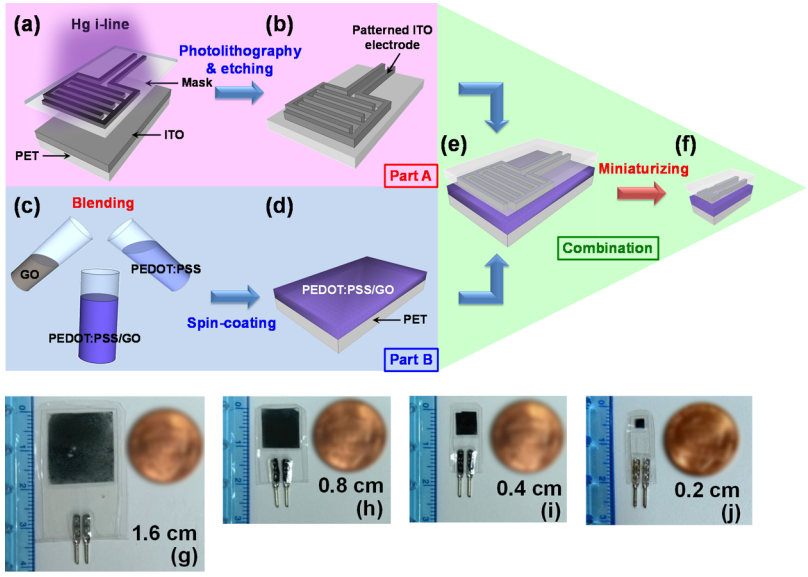

Figure 1. Fabrication procedures of piezoresistive pressure sensing devices with the IDE structure by a combination of two parts, that is, parts A and B. (a) Transferring of the scaled pattern by a conventional photolithography method; (b) chemical etching to form the ITO electrodes; (c) blending of GO and PEDOT:PSS solution with different volume ratios; (d) spin coating of the mixed solution on the O_2-plasma-treated PET substrates at a spin speed of 500 rpm to form the PEDOT:PSS/GO composite films; (e) combination of parts A and B to form the sandwich structure of pressure sensing device and packaged using a commercially available thin PET material; (f) miniaturized pressure sensing device using the scaled mask. The real-time images of the fabricated sensing devices with a cell size of (g) 1.6, (h) 0.8, (i) 0.4, and (j) 0.2 cm. The devices were placed beside a 1 cent coin of 2 cm in diameter.

water-soluble PEDOT:PSS copolymers for balancing the cationic charge of PEDOT and allowing for dispersion in water.[15,18] To enhance the performance of piezoresistive pressure sensors, some techniques have been implemented on conductive polymers. For example, nitrogen plasma was treated on the surface of PEDOT:PSS films to form sulfamate (SO_3−NH_2) and thiocyanate (S−C≡N) groups to achieve better piezoresistive characteristics.[19] In addition, gold nanoparticles have been incorporated in PEDOT:PSS films to immune the cross-talk effects of a 2 × 2 pressure-sensing array because of the increased resilience of the polymer films.[20] Pan et al. proposed applying a multiphase reaction to prepare a conductive polypyrrole with hollow-sphere microstructures for the change in contact area between the microstructured thin film and the electrodes under different pressures, resulting in an ultrahigh sensitivity at low pressure.[21]

Recently, graphene has become the most promising material composed of sp^2-hybridized carbon atoms that are bonded together in a repeating pattern of hexagons;[22] it offers many extraordinary characteristics such as the strongest, lightest, and most conductive and transparent material in the world.[23,24] Because graphene is expensive and relatively difficult to produce, some derivatives or related materials are prepared by more effective and affordable methods for various applications; for instance, plentiful and inexpensive graphene oxide (GO) with several atomic layers, which is an oxidized form of graphene with functional groups in its corner and basal planes,[25−27] might modify the conductive nature of polymer films if blended with GO. It has been reported that a GO-doped PEDOT:PSS film can act as a superior hole transport layer for high-efficiency perovskite solar cells owing to the reduction in charge recombination, enhanced charge separation and collection, and low hole-injection barrier.[28−30] For gas sensing in the environment, the large surface area of PEDOT:PSS/GO films provides a better absorption of target gas and a superior carrier transfer within the conductive polymer.[31,32] Additionally, the composite films have been employed as a contact electrode for organic light-emitting diodes,[33] energy storage such as batteries,[34] super-capacitors,[35] and thin-film transistors.[36] Nevertheless, the placement of GO flakes in PEDOT:PSS films and its effects on pressure sensing for biomedical applications are rarely investigated.

Meanwhile, scaling is primarily associated with the semiconductor industry that focuses on device miniaturization for microelectronics revolution, as described by Moore.[37,38] The scaling down of transistors for integrated circuits is widely regarded as the best method to satisfy the increasing demand for a high volume of transistors integrated into a single chip by reducing the device dimensions. When it comes to scaling for technological advances, both solid-state semiconductor and flexible electronic devices can be miniaturized, which are subjected to scaling effects.[39−41] To render pressure sensors more suitable for future biomedical applications, it is crucial to investigate the miniaturization of flexible pressure sensors. Some miniature flexible pressure sensors exist in the market; for example, the FlexiForce A101 Sensor developed by Tekscan, Inc. with a polyester substrate and a sensing area of 3.8 mm in diameter is the smallest commercial one.[42] However, the miniaturization of flexible pressure sensors and its adverse effects from scaling have not yet been investigated. In this work, we investigated the scaling effects of flexible PEDOT:PSS pressure sensors and incorporated GO into PEDOT:PSS films to solve the detrimental effects in piezoresistive characteristics under scaling. To understand the influences of GO incorporation, a morphological analysis of PEDOT:PSS/GO composite films was performed by transmission electron microscopy (TEM), field emission scanning electron microscopy (FESEM), and atomic force microscopy (AFM). Further, the chemical changes of PEDOT:PSS films blended with GO flakes were examined

DOI: 10.1021/acsami.9b10575
ACS Appl. Mater. Interfaces 2019, 11, 34305−34315

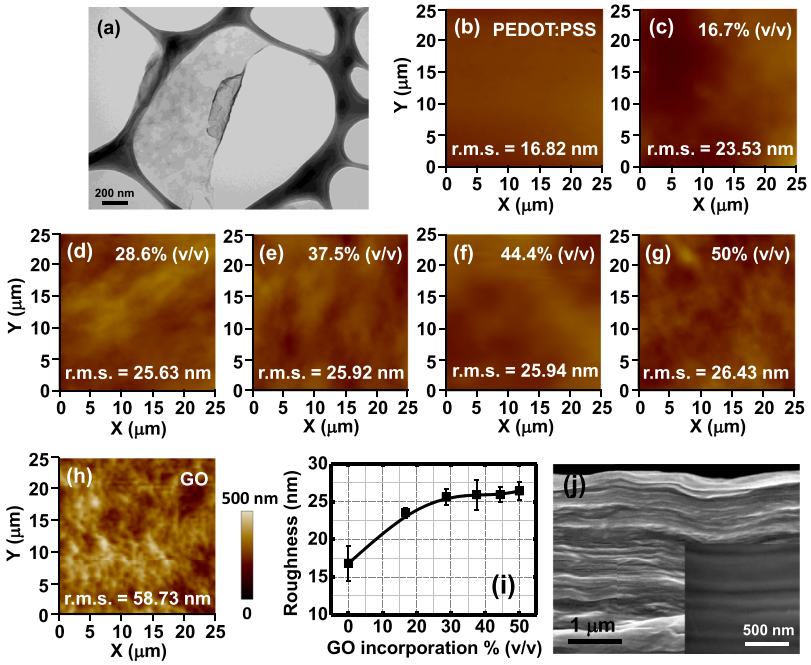

Figure 2. (a) TEM image of the GO flake on Cu grid. Topographic AFM images of (b) pure PEDOT:PSS film and PEDOT:PSS/GO composite films with a concentration of GO in (c) 16.7, (d) 28.6, (e) 37.5, (f) 44.4, and (g) 50% (v/v). The image of the pure GO film is shown in (h). (i) The statistical distribution of root-mean-square values of PEDOT:PSS/GO composite films with different concentrations of GO. (j) Cross-sectional FESEM image of the PEDOT:PSS/GO composite film with a concentration of GO in 50% (v/v). The STEM-HAADF image of the composite film is shown in the inset figure.

by X-ray photoelectron spectroscopy (XPS) and Raman spectroscopy, and the physical behaviors of the composite films were confirmed by low-temperature variable range hopping (VRH) characterization. To realize the scaling effects in piezoresistive characteristics, technology computer-aided design (TCAD) simulations were applied. Through an in vivo testing by a rat and a sound detection for a potential application in hearing aids, the prospective biomedical applications of miniaturized piezoresistive pressure sensors with PEDOT:PSS/GO composite films on flexible substrates are proposed.

MATERIALS AND METHODS

Sample Preparation. The interdigitated electrode (IDE) structure was used to fabricate the pressure-sensing devices by a combination of two parts, that is, parts A and B, where part A is the scaled and patterned indium−tin−oxide (ITO) electrode, and part B is the spin-coated PEDOT:PSS/GO composite film on a polyethylene terephthalate (PET) substrate. In this study, a 188 μm-thick flexible PET substrate covered with an ITO layer with a thickness of 0.35 μm obtained from Sigma-Aldrich Co. was used as the substrate. For part A, the transferring of the scaled pattern was performed by conventional photolithography (Figure 1a), and the ITO was etched using a mixed solution of HCl, HNO_3, and H_2O with a volume ratio of 50:3:50, as shown in Figure 1b. Meanwhile, for part B, the ITO was stripped off from the PET surface using the aforementioned solution. Subsequently, the PET substrate was cleaned with acetone and deionized (DI) water followed by O_2 plasma treatment to render the surface of a PET film hydrophilic for the spin-coating of PEDOT:PSS/GO composite films. The PEDOT:PSS solution (Clevios P VP AI 4083) with a concentration of 1.6 wt % and a resistivity of 785 Ω·cm was provided by Heraeus Holding GmbH. It is a blue-colored liquid with H_2O as a solvent. In addition, the GO solution dispersed in DI water with a concentration of 2 mg/mL was provided by Cheap Tubes Inc. The GO solution was blended into the PEDOT:PSS solution with concentrations in 16.7, 28.6, 37.5, 44.4, and 50% (v/v) and subsequently shaken vigorously for 2 min in a vortex shaker at the maximum vibration mode to mix the two solutions uniformly (Figure 1c). The mixed solution was spin-coated on the O_2 plasma-treated PET substrates at a spin speed of 500 rpm and baked at 120 °C for 20 min in the atmosphere to evaporate the excess water and to increase the resiliency of the fabricated PEDOT:PSS/GO composite films, as shown in Figure 1d. The thickness of these films was approximately 1.88 μm, which is the same as those of our previous studies.[19,20,43] Finally, parts A and B were combined to form a sandwich structure and packaged using a commercially available thin PET material to reduce the issues emerging from the less intimate contact between the scaled ITO electrode and the composite films (Figure 1e). All the scaled devices, as shown in Figure 1f, were fabricated using the scaled masks designed by a computer-aided design tool (AutoCAD) with a scaling factor of 2 (Figure S1 of the Supporting Information). All the fabricated devices were annotated with the common electrode length, that is, 1.6, 0.8, 0.4, and 0.2 cm. More detailed fabrication procedures of the pressure-sensing devices can be obtained from our previous studies.[43]

Characterization. To confirm the size of GO flakes, the Cu grid was used to hold the flakes and subsequently investigated by TEM (FEI Tecnai F20, FEI Company). Besides, the morphological and cross-sectional analyses of the PEDOT:PSS/GO composite films were performed by AFM (Bruker AXS MultiMode 8, Bruker Corp.), FESEM (JSM-7500F, JEOL Ltd.) and TEM. To investigate the chemical composition, the PEDOT:PSS films blended with GO flakes were examined by XPS (VG ESCA Scientific Theta Probe, Fisher Scientific International, Inc.) and Raman spectroscopy (Micro Raman/PL/TR-PL spectrometer, ProTrustech Co., Ltd.). The Hall mobility was measured by a Hall affect analyzer (AHM-800B, Agilent Technologies) with van der Pauw's configuration. For the electrical characterization, the fabricated pressure sensors were first placed on a homemade sample holder made of rigid steel, and the pressure was applied by a vertical stand equipped with a force gauge (JSV-H1000 Vertical Servo Stand, ALGOL Instrument Co., Ltd.) through an aluminum tip. Because an equal pressure should be applied on all the sensors, a square quartz layer of 1 cm^2 was inserted between the aluminum tip and sensors. Pressures ranging from 0.1 to 20 kPa were

DOI: 10.1021/acsami.9b10575
ACS Appl. Mater. Interfaces 2019, 11, 34305−34315

applied at a rate of 2 mm/s for the analysis of the piezoresistive behaviors. The electrical characteristics of the fabricated piezoresistive pressure sensors were analyzed by using a Keithley 2450 Interactive Digital SourceMeter (Keithley Instruments Inc.). The left and right electrodes were biased at 2 and −2 V, respectively, and the resistance of the pressure sensors was directly measured under the pressure applied. Moreover, the VRH measured by a cryogenic prober station (CG-196CU, EverBeing International Corp.) was performed to investigate the change in carrier transportation, and a TCAD simulation (Sentaurus, Synopsys, Inc., 2013.12 Release) was performed to obtain the distribution of current density in the scaled piezoresistive pressure sensors with PEDOT:PSS/GO composite films.

RESULTS AND DISCUSSION

Material Analyses of PEDOT:PSS Films Blended with GO Flakes. The real-time images of the fabricated sensing devices with a cell size of 1.6−0.2 cm are shown in Figure 1g−j. The devices were placed beside a 1 cent coin of 2 cm in diameter. In these photographs, a general comprehension regarding the size of our miniaturized sensing devices can be obtained, where the largest device of 1.6 cm can cover almost the entire coin, whereas the smallest one of 0.2 cm is less than one-eighth of the coin. Figure 2a shows the TEM image of the GO flake used in this study. The size of the flake is in the micrometer range, which is in the same order of magnitude compared with the film thickness. Figure 2b−g shows the topographic images of the pure PEDOT:PSS film and PEDOT:PSS/GO composite films obtained by AFM with a field of view of 25 μm × 25 μm. The surface roughness of the composite films is shown in these images and found to be approximately 23−26 nm, which is slightly increased compared to that of the pure PEDOT:PSS film but much smaller than that of the GO film, as shown in Figure 2h,i. Figure 2j shows the cross-sectional FESEM image of the PEDOT:PSS/GO composite film with a concentration of GO in 50% (v/v). The scanning transmission electron microscope high-angle annular dark-field (STEM-HAADF) image of the composite film was also obtained and is presented in the inset of this figure. The cross-sectional FESEM, TEM, and STEM-HAADF images of the pure PEDOT:PSS film are shown in Figures S2 and S3 of the Supporting Information, and the images of the PEDOT:PSS/GO composite film with the same scale bar are also included for the purpose of comparison. To clearly observe the GO flakes within the PEDOT:PSS film, a spin coating speed of 300 rpm was applied to achieve a thicker film thickness of approximately 5 μm. Compared to those of the pure PEDOT:PSS film, the images of the PEDOT:PSS/GO composite film with a concentration of GO in 50% (v/v) exhibit distinct GO flakes that are placed horizontally in PEDOT:PSS copolymers, modifying the piezoresistive behaviors of the pressure sensors, which will be discussed later.

The material change in the PEDOT:PSS films blended with GO flakes was confirmed by XPS and Raman spectroscopy. For the XPS analysis, the C 1s and O 1s spectra of all samples were examined and are shown in Figure 3a. The XPS spectra were adjusted by the position of the primary C 1s (C−C) peak at the binding energy of 284.6 eV.[44] For the C 1s spectra of the pure PEDOT:PSS film, three primary deconvoluted peaks can be obtained at 284.6, 285.1, and 286.5 eV, belonging to the C−C, C−S, and C−O−C bonds, respectively.[45] An additional peak appearing at 285.8 eV that belongs to the C−O−H bond can be observed from the PEDOT:PSS films blended with GO flakes, as proposed by Ganguly et al.[46] The intensity of the C−S peak for all fabricated samples is approximately the same because the sulfur atoms are only from the PEDOT:PSS film, as shown in Figure S4a of the Supporting Information; thus, the C−S peak can be treated as the reference peak for the calculation of the peak-to-area ratios (PARs). Then, the PARs for the C−O−H, C−C, and C−O−C peaks with respect to the C−S peak were calculated and are shown in Figures 3b and S4b,c of the Supporting Information, respectively. In these figures, a significant increment in PARs of the C−O−H, C−C, and C−O−C bonds with respect to the reference C−S bond is observed for the samples with the increase in GO

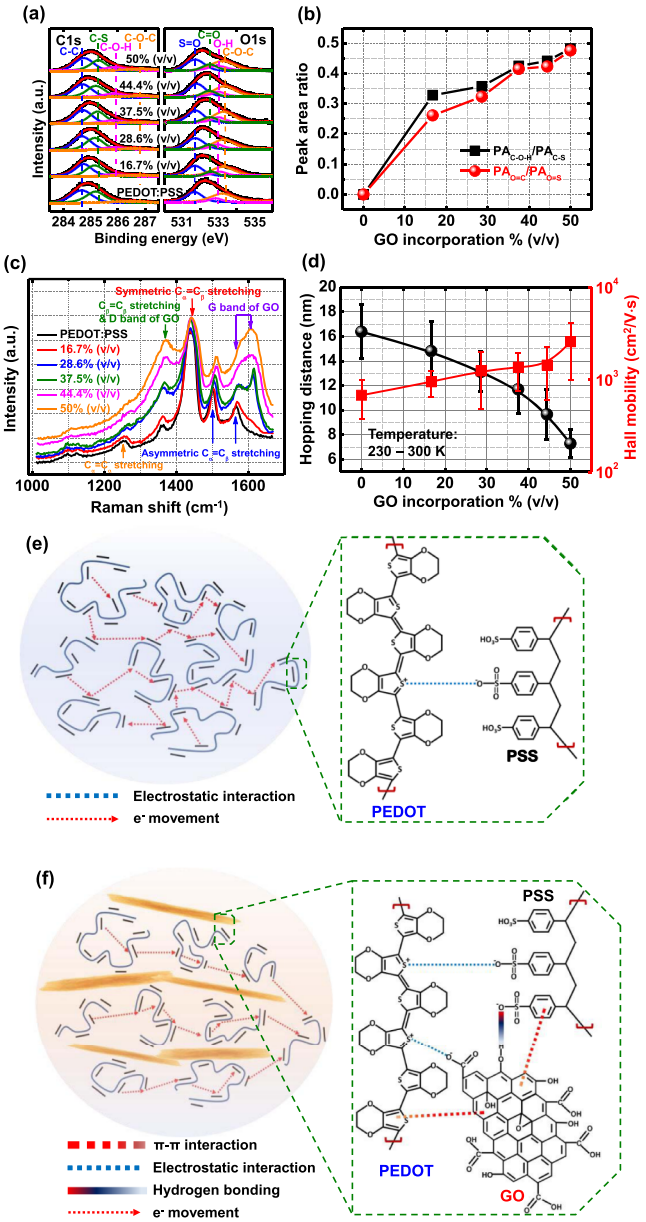

Figure 3. (a) C 1s and O 1s XPS spectra of PEDOT:PSS/GO composite films with different concentrations of GO. (b) PARs of the C−O−H and O═C peaks with respect to the C−S and O═S peaks, respectively. (c) Raman spectra of PEDOT:PSS/GO composite films with different concentrations of GO. (d) VRH distance and Hall mobility of the pure PEDOT:PSS film and PEDOT:PSS films blended with GO flakes. The schematic diagrams of carrier transportation and chemical structure of (e) pure PEDOT:PSS and (f) PEDOT:PSS/GO composite films.

DOI: 10.1021/acsami.9b10575
ACS Appl. Mater. Interfaces 2019, 11, 34305−34315

incorporation ratio. In addition, the deconvolution of the O 1s peak was performed and is shown in Figure 3a. Three major sub-peaks can be observed at 531.8, 533, and 533.4 eV in all PEDOT:PSS and PEDOT:PSS/GO composite films, corresponding to the S═O, O−H, and C−O−C bonds, respectively.[47,48] For the PEDOT:PSS films blended with GO flakes, the presence of a new peak around 532.5 eV that belongs to the O═C bond is found.[49] A similar analysis of the PARs for the O 1s sub-peaks was performed. The S═O peak can be considered as the reference peak with a constant peak intensity of all samples (Figure S5a of the Supporting Information). Based on the reference peak of the S═O bond, the PARs for the O═C, C−O−C, and O−H bonds were calculated and enhanced with the increase in GO incorporation ratio, as shown in Figures 3b and S5b,c of the Supporting Information. The increasing intensity of oxygen along with carbon containing peaks is the indication of a successful incorporation of GO flakes into PEDOT:PSS films.

Figure 3c presents the Raman spectra of the pure PEDOT:PSS film and PEDOT:PSS/GO composite films. The primary bands in this figure are symmetric C_α═C_β stretching vibrations at 1436−1442 cm^{-1}, asymmetric C_α═C_β stretching vibrations from the thiophene rings in the middle and the end of the PEDOT chains at 1498−1500 and 1591−1610 cm^{-1}, respectively, and C_β−C_β stretching vibrations at 1362−1365 cm^{-1}.[50−53] For the pure PEDOT:PSS film, the Raman peaks of symmetric C_α═C_β stretching, asymmetric C_α═C_β stretching from the thiophene rings in the middle of the PEDOT chains, and C_α−C_α inter-ring vibrations are at 1436, 1498, and 1256 cm^{-1}, respectively. With the increase in GO incorporation ratio of the PEDOT:PSS/GO composite films, these three peaks shift to higher wave numbers of 1442, 1512, and 1263 cm^{-1}, respectively, which can be attributed to a shorter bond length with higher vibrational frequencies.[54,55] The change in bond length is caused by the $\pi-\pi$ interaction between the thiophene ring of PEDOT and GO flakes.[51] Furthermore, the increased intensity of the Raman spectra at 1362−1365 and 1591−1610 cm^{-1}, belonging to D and G bands of GO, respectively, as confirmed by the Raman spectra of GO in Figure S6 of the Supporting Information, proves the presence of GO flakes in the PEDOT:PSS films. The D-band is from the structural disorder and defects induced by the sp^2-hybridization, and the G-band represents the planar configuration of the sp^2-bonded carbon in the two-dimensional hexagonal lattice of GO flakes. Figure 3d displays the VRH distance and Hall mobility of the pure PEDOT:PSS film and PEDOT:PSS films blended with GO flakes. We used the temperature-dependent conductance, $G(T)$, of the PEDOT:PSS/GO composite films described by Mott's law to determine the hopping distance, as shown in the following[56]

$$G(T) = G_0\left[-\left(\frac{T_0}{T}\right)^{\gamma}\right] \tag{1}$$

where G_0 is the prefactor of the conductance, T_0 is the characteristic temperature, T is the measurement temperature from 230 to 300 K, and γ is the power component of (T_0/T) that is related to the transport process of carriers in PEDOT:PSS/GO composite films. Here, the value of γ is suggested to be $1/(d+1)$, where d is the dimensionality and equals 3 for a three-dimensional (3D) VRH.[57] To extract the values of T_0, the conductance of the films at each of the temperatures was measured for the linear fitting of the $G-T^{-1/4}$ curves, as shown in Figure S7 of the Supporting Information. The extracted T_0 is a function of the density of states at the Fermi level, $N(E_F)$, which is described in the following equation

$$T_0 = \frac{\beta}{N(E_F)\xi^3 k_B} \tag{2}$$

where ξ is the localization length, β is a numerical coefficient with the value of 21.2 provided by Efros et al.,[58] and k_B is the Boltzmann constant. Subsequently, we can obtain $N(E_F)$ from T_0 to extract the hopping distance (l_0) as shown in eq 3[59]

$$l_0 = \left\{\frac{3}{2\alpha\left(\frac{4\pi}{3}\right)N(E_F)k_B T}\right\}^{1/4} \tag{3}$$

where α is the decay rate of the wave function and equals $1/\xi$.[60] As shown in Figure 3d, the PEDOT:PSS films blended with GO flakes demonstrate the hopping distance of 7.3−14.4 nm, which is lower than that of the pure PEDOT:PSS film. The reduced hopping distance of the PEDOT:PSS/GO composite films is ascribed to the $\pi-\pi$ interaction between the thiophene ring of PEDOT and GO flakes for a shorter bond length, as revealed in the Raman spectra of Figure 3c. The decrease in the hopping distance value also results in a high carrier mobility of the composite films with an increase in GO volume percentage, thus enhancing the conductivity of the PEDOT:PSS films. The Hall mobility (μ) of the PEDOT:PSS/GO composite films obtained in Figure 3d was measured by employing the van der Pauw method using the following relationship[61−64]

$$\mu = \frac{d \times \Delta R_H}{B \times \rho} \tag{4}$$

where d is the PEDOT:PSS/GO composite film thickness, ΔR_H is the resistance change with the applied magnetic field (B) of 0.4 T, and ρ is the resistivity of the film. Figure 3e,f illustrates the schematic diagrams of the carrier transportation and chemical structure of the pure PEDOT:PSS and PEDOT:PSS/GO composite films, respectively. For the PEDOT:PSS film blended with GO flakes, the $\pi-\pi$ interaction between the thiophene ring of PEDOT and GO flakes, the electrostatic interaction between PEDOT cations and GO anions, and the hydrogen bonding between PSS and GO flakes are observed. They modify the thiophene backbone of the PEDOT:PSS chains by reducing the distance between two hopping sites in a highly amorphous PEDOT:PSS/GO composite film for a high carrier conductivity. Moreover, with the horizontal placement of GO flakes in PEDOT:PSS copolymers, an uniform electron movement in the PEDOT:PSS/GO composite film occurs.

Piezoresistive Behaviors of Miniaturized Pressure Sensors. The typical piezoresistive pressure-sensing characteristics of the fabricated PEDOT:PSS films blended with different GO concentrations for the device sizes of 1.6 and 0.2 cm are illustrated in Figure 4a through a resistance versus pressure ($R-P$) curve. Samples with different GO concentrations for the device sizes of 0.8 and 0.4 cm were also measured, and the characteristics are shown in Figure S8 of the Supporting Information. To obtain the statistical distribution in $R-P$ curves, at least 10 samples were characterized. As shown, with the increase in GO volume percentage, the

DOI: 10.1021/acsami.9b10575
ACS Appl. Mater. Interfaces 2019, 11, 34305−34315

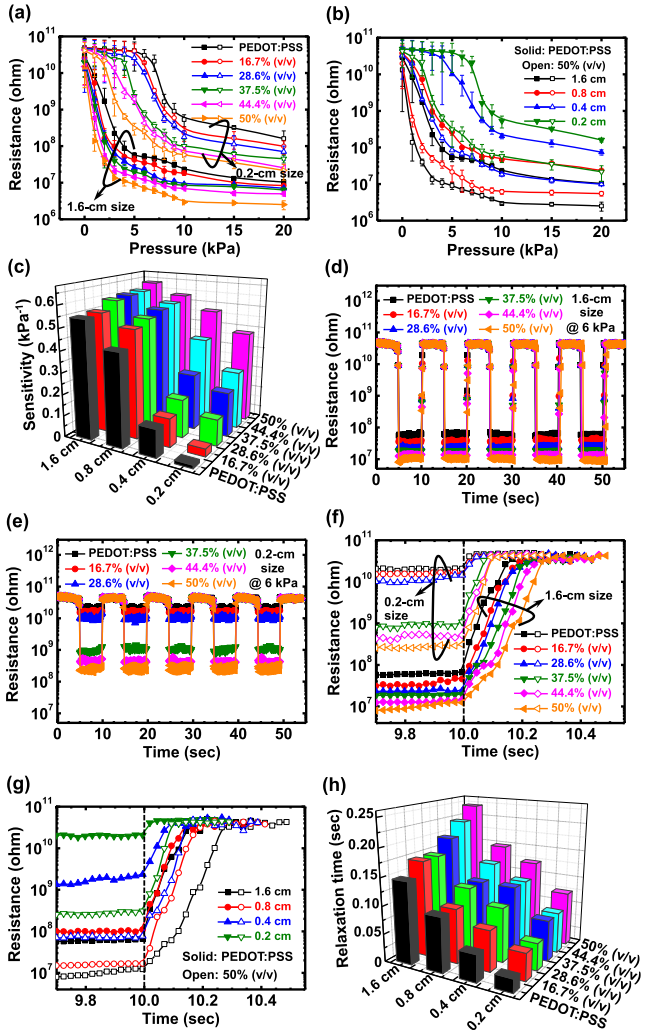

Figure 4. $R-P$ curves of PEDOT:PSS/GO piezoresistive pressure sensors with (a) different concentrations of GO for the device sizes of 0.2 and 1.6 cm, and (b) different device sizes for the concentrations of GO in 0 and 50% (v/v). (c) 3D matrix in sensitivity of PEDOT:PSS/GO piezoresistive pressure sensors with different concentrations of GO and device sizes. Reversible testing characteristics of loading/unloading cycles for (d) 1.6 and (e) 0.2 cm piezoresistive pressure sensors with PEDOT:PSS/GO composite films. $R-t$ curves of PEDOT:PSS/GO piezoresistive pressure sensors with (f) different concentrations of GO for the device sizes of 0.2 and 1.6 cm, and (g) different device sizes for the concentrations of GO in 0 and 50% (v/v). (h) 3D matrix in relaxation time of PEDOT:PSS/GO piezoresistive pressure sensors with different concentrations of GO and device sizes.

resistance of the pressure sensors decreases significantly. However, when the device dimension is reduced to 0.2 cm, a distinct late response in pressure of the $R-P$ curves for the samples with the pure PEDOT:PSS film is observed, as shown in the piezoresistive characteristics of the PEDOT:PSS films blended with different GO concentrations for different sizes (Figures 4b and S9 of the Supporting Information). This issue can be solved by GO incorporation because the GO flakes can provide a uniform electron movement in PEDOT:PSS copolymers, as revealed in Figure 3f. Furthermore, the piezoresistive sensitivity of these samples was calculated from the slopes of the $R-P$ curves at a pressure lower than 6 kPa that is the critical point of the pressure to avoid brain tissue damage during the intracranial surgery of a rat and will be discussed later. The sensitivity was calculated according to eq 5,[43] and the results are displayed in a 3D matrix format in Figure 4c.

$$S = \frac{\log(R_0) - \log(R_{6\text{kPa}})}{6\ \text{kPa}} \tag{5}$$

where S is the piezoresistive sensitivity, R_0 is the resistance when no pressure is applied, and $R_{6\text{kPa}}$ is the resistance when a pressure of 6 kPa is applied. For the devices with pure PEDOT:PSS films, the piezoresistive sensitivity decreases significantly with the scaling of the devices. Fortunately, an increment in sensitivity with the increase in GO incorporation ratio can be obtained. For the devices with a cell size of 0.2 cm, the sensitivity of the samples with PEDOT:PSS/GO composite films increases from 0.016 to 0.428 kPa^{-1}, suitable for biomedical applications. The highest piezoresistive sensitivity of 0.548 kPa^{-1} is achieved for a 1.6 cm device with the PEDOT:PSS film blended with a concentration of GO in 50% (v/v).

Figure 4d,e shows the reversible testing characteristics of loading/unloading cycles for the 1.6 and 0.2 cm piezoresistive pressure-sensing devices, respectively, with PEDOT:PSS/GO composite films. The cycling behaviors for the 0.4 and 0.8 cm devices were also measured and are demonstrated in Figure S10a,b of the Supporting Information, respectively. A pressure of 6 kPa was applied for 5 s and subsequently released for 5 s. A stable resistive switching is observed for all fabricated samples with different structures and materials. To further investigate the time-dependent piezoresistive response, the resistance versus time ($R-t$) curves of the piezoresistive pressure sensors with different GO incorporation ratios are displayed in Figures 4f and S10c,d of the Supporting Information. The relaxation time (t_r) is defined as the time required to reach the high resistance of 30 GΩ after the pressure is released, which can be calculated using the following equation

$$t_r = t_2 - t_1 \tag{6}$$

where t_2 is the time required for the resistance to reach a high resistance of 30 GΩ, and t_1 is the time when the pressure is released. In these figures, a longer relaxation time can be observed in samples with higher GO incorporation ratios because of the lower resistance of the sensors under the pressure applied. In addition, a scaled device presents a shorter relaxation time, as shown in Figures 4g and S11 of the Supporting Information; it can be applied in biomedical applications such as the detection of sound vibrations and will be presented later. We have compared the relaxation time of all fabricated samples in a 3D matrix, as shown in Figure 4h. It is found that the relaxation time is slightly longer for larger devices, especially the samples with high GO incorporation ratios. If we consider the sensitivity and time-response simultaneously for a specific size of a piezoresistive pressure sensor, the GO incorporation ratio should be optimized. For example, for a 0.4 cm device, the PEDOT:PSS film blended with a concentration of GO in 44.4% (v/v) would be the optimized condition for better piezoresistive sensing behaviors.

To obtain a physical insight into the late response in pressure of the $R-P$ curves for the scaled devices with the pure PEDOT:PSS film, as shown in Figure 4a,b, we performed a current density simulation of the large (1.6 cm) and scaled (0.2 cm) devices with the pure PEDOT:PSS film and PE-

DOI: 10.1021/acsami.9b10575
ACS Appl. Mater. Interfaces 2019, 11, 34305−34315

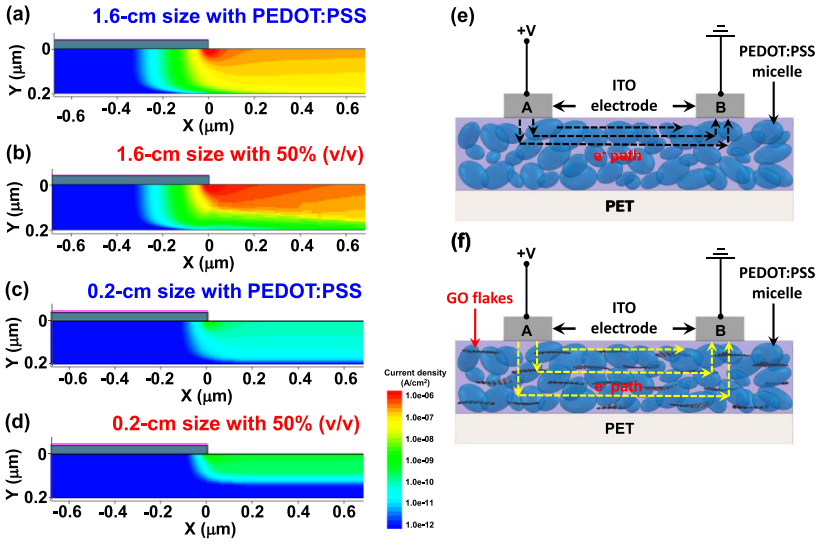

Figure 5. Current−density simulation of piezoresistive pressure sensors with (a) pure PEDOT:PSS film and (b) PEDOT:PSS/GO composite film with a concentration of GO in 50% (v/v) for a 1.6 cm size, and with (c) pure PEDOT:PSS film and (d) PEDOT:PSS/GO composite film with a concentration of GO in 50% (v/v) for a 0.2 cm size. Theoretical models in carrier transportation of the piezoresistive pressure sensors with (e) pure PEDOT:PSS and (f) PEDOT:PSS/GO composite films.

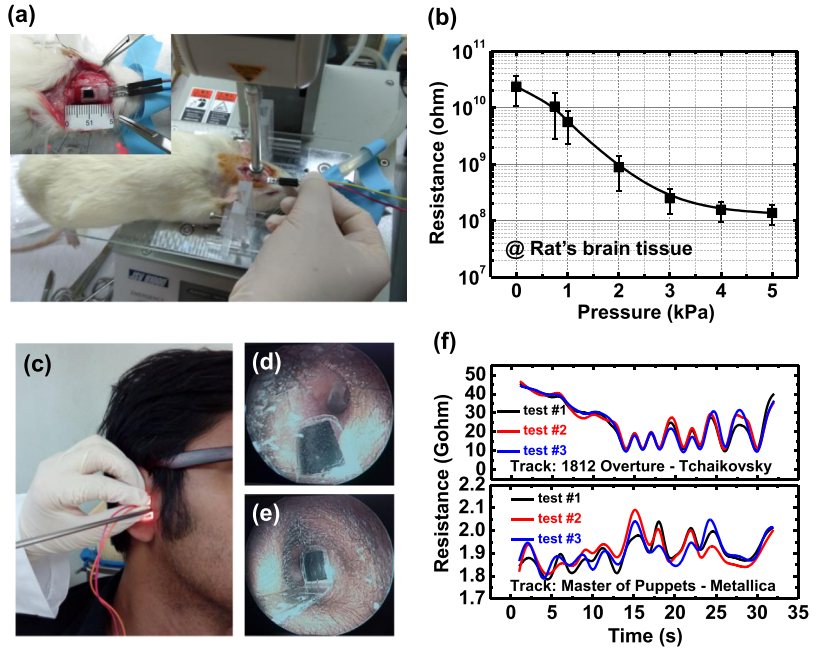

Figure 6. (a) Real-time photograph of intracranial surgery of a rat with the fabricated PEDOT:PSS/GO pressure sensor. (b) *R*−*P* curve of the fabricated pressure sensor on the rat's brain surface without creating any major damage. (c) Photograph of the testing for the detection of sound vibrations with the fabricated PEDOT:PSS/GO piezoresistive pressure sensor and an ear endoscope. The photographs of the fabricated pressure sensor (d) in the ear canal and (e) covered on the ear drum. (f) Detecting signals of different styles of music, that is, classical and heavy metal music, respectively.

DOT:PSS/GO composite film with a concentration of GO in 50% (v/v). In our previous study,[43] the piezoresistive pressure-sensing devices used in this work, that is, the IDE structure, exhibited a horizontal conducting path. Besides, the pressure sensors with a cross-point electrode (CPE) structure presented a vertical conduction. Using the resistance values obtained from the pressure sensors with IDE and CPE structures as shown in Figures 4a and S12a of the Supporting Information, respectively, the vertical and horizontal resistivities of the pure PEDOT:PSS film and PEDOT:PSS/GO composite films with different GO concentrations were extracted. Subsequently, the vertical to horizontal resistivity ratio ($\rho_{vertical}/\rho_{horizontal}$) was calculated to understand the change in electron movement of the PEDOT:PSS/GO composite films, as displayed in Figure S12b of the Supporting Information. With the increase in GO incorporation ratio, the $\rho_{vertical}/\rho_{horizontal}$ is smaller, implying that the electron movement in PEDOT:PSS/GO composite films becomes more uniform. The resistivity data were used to simulate the current density of the large and scaled pressure sensors with the pure PEDOT:PSS film and PEDOT:PSS/GO composite film with a concentration of GO in 50% (v/v), as shown in Figure 5a−d. The biases of the left and right

DOI: 10.1021/acsami.9b10575
ACS Appl. Mater. Interfaces 2019, 11, 34305−34315

electrodes are 2 and −2 V, respectively. For the devices with the pure PEDOT:PSS film, the current crowded at the electrode corner is significant (Figure 5a,c), thus resulting in a high resistance value of the scaled pressure sensors under the pressure applied (Figure 4a,b), as revealed in semiconductor devices such as vertical power bipolar junction transistors.[65] It is noteworthy that the current density in devices becomes more uniform for the PEDOT:PSS films blended with GO (Figure 5b,d), thus eliminating the late response in pressure of the $R-P$ curves for the scaled devices. For the devices with the same composition of PEDOT:PSS/GO films, the current crowding effect at the electrode corner would become more significant when the size of the IDE electrode scales.[66,67] The current crowding introduces an additional serious resistance at the electrode, responsible for the late response and decreased sensitivity of the scaled devices. A theoretical model is proposed to explain the carrier transportation of the piezoresistive pressure sensors with the pure PEDOT:PSS film and PEDOT:PSS/GO composite films presented in Figure 5e,f, respectively. In general, a PEDOT:PSS film consists of PEDOT-rich cores with a high intrinsic conductivity and a PSS-rich shell with a weak ionic conductor. Hence, for a pure PEDOT:PSS film, a high resistivity in the vertical conducting path is observed because the PEDOT-rich domains are separated by thick PSS-lamella barriers, contributing to a nonuniform current distribution of PEDOT:PSS films for the piezoresistive pressure sensors with the IDE structure, especially the current crowding effect at the surface of the film and in the vicinity of an ITO electrode corner, as illustrated in Figure 5e. Meanwhile, for the PEDOT:PSS/GO composite films, a reduced resistivity in the vertical conducting path is achieved, resulting in a uniform electron movement between electrodes (Figure 5f).

Biomedical Applications of Miniaturized Piezoresistive Pressure Sensors. Figure S13 of the Supporting Information demonstrates the repeatability behavior of the 0.2 cm piezoresistive pressure sensor with the PEDOT:PSS/GO composite film with a concentration of GO in 50% (v/v). A pressure of 6 kPa was applied on the device and then released. It is found that the scaled device can maintain a stable loading/unloading operation for more than 300 cycles. Considering the properties of good sensitivity, excellent response, and high repeatability of the piezoresistive pressure sensors with PEDOT:PSS/GO composite films, the miniaturized one should be the ideal candidate for future biomedical applications such as the pressure monitoring during surgery and the detection of sound vibrations. Figure 6a shows the real-time photograph of intracranial surgery of a rat with a PEDOT:PSS/GO pressure sensor. In this experiment, we used the pressure sensor with a device size of 0.2 cm that fitted perfectly in the window created in the skull of a fully grown male rat, as shown in the photograph in the inset figure. The pressure was applied on the opened window through the device, and the pressure was limited to 5 kPa to avoid inducing any damage on rat's brain. As shown in Figure 6b, our miniaturized pressure sensors are suitable for sensing the pressure on rat's brain surface without creating any major damage. Figure 6c−e shows the detection of sound vibrations for a potential application in hearing aids. The pressure sensors with a device size of 0.2 cm can be fitted inside the human ear because the size of an ear drum is approximately the same as that of our device, as revealed in Figure 6e. For the application in hearing aids, if the miniaturized pressure-sensing device can be implanted into ear, it can help the patient to detect sound without any additional accessories. The behaviors of our fabricated device inside a human ear to sense sound vibrations are presented in this work and illustrated in Figure 6f for the detection of different styles of music, that is, classical and heavy-metal music. For classical music, we used a 30 s track from Tchaikovsky's 1812 Overture and found that the periodic cannon-shots were detected by our sensor as the resistance decreased instantly and subsequently returned to a higher resistance according to the cannon-shot; this was repeated for three times. For heavy-metal music, we selected a 30 s track from the Master of Puppets by Metallica and observed a relatively lower resistance throughout the response curves because of the heavy drumming detected by the pressure sensor. From these investigations, it is evident that the miniaturized piezoresistive pressure sensors with PEDOT:PSS/GO composite films are promising for biomedical applications.

CONCLUSIONS

In this study, miniaturized piezoresistive pressure sensors with PEDOT:PSS/GO composite films were developed. PEDOT:PSS films blended with different amounts of GO flakes were identified using morphological investigations by TEM, FESEM, and AFM imaging and chemical analyses by XPS and Raman spectroscopy. By examining the low-temperature current versus voltage ($I-V$) characteristics, a reduced VRH distance was found, owing to the horizontal placement of GO flakes within the PEDOT:PSS films. For a PEDOT:PSS pressure sensor scaled to 0.2 cm, a late response was observed, thus resulting in a reduced piezoresistive sensitivity. The detrimental scaling effect was found to result from the current crowded at the PEDOT:PSS film surface and in the vicinity of an ITO electrode corner, as proven by TCAD simulations, and can be solved effectively by GO incorporation. For the prospective biomedical applications of miniaturized piezoresistive pressure sensors with PEDOT:PSS/GO composite films, the brain pressure monitoring of a rat under intracranial surgery and the discernment of different styles of music have been demonstrated.

ASSOCIATED CONTENT

Supporting Information

The Supporting Information is available free of charge on the ACS Publications website at DOI: 10.1021/acsami.9b10575.

Layouts of piezoresistive pressure sensors for different device sizes; cross-sectional FESEM, TEM, and STEM-HAADF images of the pure PEDOT:PSS film and the PEDOT:PSS/GO composite film with the concentration of GO in 50% (v/v); C−S peak area in C 1s XPS spectra and PARs for C−C and C−O−C peaks with respect to the C−S peak of PEDOT:PSS/GO composite films; S═O peak area in O 1s XPS spectra and PARs for C−O−C and O−H peaks with respect to the S═O peak of PEDOT:PSS/GO composite films; Raman spectra of GO; linear fitting of $G-T^{-1/4}$ curves for the PEDOT:PSS/GO composite films; $R-P$ curves of PEDOT:PSS/GO piezoresistive pressure sensors for the device sizes of 0.8 and 0.4 cm; $R-P$ curves of PEDOT:PSS/GO piezoresistive pressure sensors with the concentrations of GO in 16.7−44.4% (v/v); reversible testing characteristics of loading/unloading

DOI: 10.1021/acsami.9b10575
ACS Appl. Mater. Interfaces 2019, 11, 34305−34315

cycles for 0.4 and 0.8 cm piezoresistive pressure sensors and $R-t$ curves of piezoresistive pressure sensors for the device sizes of 0.4 and 0.8 cm; $R-t$ curves of PEDOT:PSS/GO piezoresistive pressure sensors with the concentrations of GO in 16.7−44.4% (v/v); $R-P$ curves of PEDOT:PSS/GO piezoresistive pressure sensors with different concentrations of GO for the CPE structure and vertical to horizontal resistivity ratio ($\rho_{vertical}/\rho_{horizontal}$) of the PEDOT:PSS/GO composite films with different concentrations of GO; and repeatability behavior of the 0.2 cm piezoresistive pressure sensor with the PEDOT:PSS/GO composite film with a concentration of GO in 50% (v/v) (PDF)

AUTHOR INFORMATION

Corresponding Authors

*E-mail: jcwang@mail.cgu.edu.tw. Phone: +886-3-2118800 ext. 5784. Fax: +886-3-2118507 (J.-C.W.).
*E-mail: alexlu0416@gmail.com. Phone: +886-968371883. Fax: +886-3-3285818 (Y.-J.L.).

ORCID

Jer-Chyi Wang: 0000-0002-1308-3197
Ming-Chung Wu: 0000-0002-3584-3871

Notes

The authors declare no competing financial interest.

ACKNOWLEDGMENTS

This research was supported by the Ministry of Science and Technology, R.O.C (contract nos. of MOST 107-2218-E-182-007 and MOST 108-2218-E-182-003) and Chang Gung Memorial Hospital, Linkou, Taiwan (contract nos. of CMRPD2F0123, CMRPD2H0131, and BMRPA74). The authors would like to thank Dr. Ruey-Dar Chang and Mr. Song-Hong Lin, Chang Gung University, Taiwan, and Dr. Pi-Chun Juan and Dr. Jyh-Wei Lee, Ming Chi University of Technology, Taiwan, for their technical supports.

REFERENCES

(1) Kweon, O. Y.; Lee, S. J.; Oh, J. H. Wearable High-Performance Pressure Sensors Based on Three-dimensional Electrospun Conductive Nanofibers. *NPG Asia Mater.* **2018**, *10*, 540−551.
(2) Giovanelli, D.; Farella, E. Force Sensing Resistor and Evaluation of Technology for Wearable Body Pressure Sensing. *J. Sens.* **2016**, *2016*, 1−13.
(3) Chatzandroulis, S.; Goustouridis, D.; Normand, P.; Tsoukalas, D. A Solid-State Pressure-Sensing Microsystem for Biomedical Applications. *Sens. Actuators, A* **1997**, *62*, 551−555.
(4) Cheng, M.-Y.; Lin, C.-L.; Lai, Y.-T.; Yang, Y.-J. A Polymer-Based Capacitive Sensing Array for Normal and Shear Force Measurement. *Sensors* **2010**, *10*, 10211−10225.
(5) Maudie, T.; Wertz, J. Pressure Sensor Performance and Reliability. *IEEE Trans. Ind. Appl.* **1997**, *3*, 37−43.
(6) Ngo, H. D.; Mackowiack, P.; Grabbert, N.; Weiland, T.; Hu, X.; Schneider-Ramelow, M.; Ehrmann, O.; Lang, K. D. *The Roadmap for Development of Piezoresistive Micro Mechanical Sensors for Harsh Environment Applications. 2017 Eleventh International Conference on Sensing Technology (ICST)*, Sydney, NSW, 2017; Vol. *1*−*6*.
(7) Fiorillo, A. S. A Piezoresistive Tactile Sensor. *IEEE Trans. Instrum. Meas.* **1997**, *46*, 15−17.
(8) Blasquez, G.; Chauffleur, X.; Pons, P.; Douziech, C.; Favaro, P.; Menini, P. Intrinsic Thermal Behaviour of Capacitive Pressure Sensors: Mechanisms and Minimisation. *Sens. Actuators, A* **2000**, *85*, 65−69.
(9) Tressler, J. F.; Alkoy, S.; Newnham, R. E. Piezoelectric Sensors and Sensor Materials. *J. Electroceram.* **1998**, *2*, 257−272.
(10) Wisitsoraat, A.; Patthanasetakul, V.; Lomas, T.; Tuantranont, A. Low cost thin film based piezoresistive MEMS tactile sensor. *Sens. Actuators, A* **2007**, *139*, 17−22.
(11) Barlian, A. A.; Park, W.-T.; Mallon, J. R.; Rastegar, A. J.; Pruitt, B. L. Review: Semiconductor Piezoresistance for Microsystems. *Proc. IEEE* **2009**, *97*, 513−552.
(12) Latessa, G.; Brunetti, F.; Reale, A.; Saggio, G.; Di Carlo, A. Piezoresistive behaviour of flexible PEDOT:PSS based sensors. *Sens. Actuators, B* **2009**, *139*, 304−309.
(13) Trifigny, N.; Kelly, F.; Cochrane, C.; Boussu, F.; Koncar, V.; Soulat, D. PEDOT:PSS-Based Piezo-resistive Sensors Applied to Reinforcement Glass Fibres for in situ Measurement During the Composite Material Weaving Process. *Sensors* **2013**, *13*, 10749−10764.
(14) Lang, U.; Rust, P.; Schoberle, B.; Dual, J. Piezoresistive properties of PEDOT:PSS. *Microelectron. Eng.* **2009**, *86*, 330−334.
(15) Ding, Y.; Yang, J.; Tolle, C. R.; Zhu, Z. Flexible and Compressible PEDOT:PSS@Melamine Conductive Sponge Prepared via One-Step Dip Coating as Piezoresistive Pressure Sensor for Human Motion Detection. *ACS Appl. Mater. Interfaces* **2018**, *10*, 16077−16086.
(16) Takano, T.; Masunaga, H.; Fujiwara, A.; Okuzaki, H.; Sasaki, T. PEDOT Nanocrystal in Highly Conductive PEDOT:PSS Polymer Films. *Macromolecules* **2012**, *45*, 3859−3865.
(17) Li, Z.; Qin, F.; Liu, T.; Ge, R.; Meng, W.; Tong, J.; Xiong, S.; Zhou, Y. Optical Properties and Conductivity of PEDOT:PSS Films Treated by Polyethylenimine Solution for Organic Solar Cells. *Org. Electron.* **2015**, *21*, 144−148.
(18) Skotheim, T.; Reynolds, J. *Handbook of Conducting Polymers*, 3rd ed.; CRC Press: New York, USA, 2007.
(19) Wang, J.-C.; Karmakar, R. S.; Lu, Y.-J.; Wu, M.-C.; Wei, K.-C. Nitrogen Plasma Surface Modification of Poly(3,4-ethylenedioxythiophene):Poly(styrenesulfonate) Films To Enhance the Piezoresistive Pressure-Sensing Properties. *J. Phys. Chem. C* **2016**, *120*, 25977−25984.
(20) Karmakar, R. S.; Lu, Y.-J.; Fu, Y.; Wei, K.-C.; Chan, S.-H.; Wu, M.-C.; Lee, J.-W.; Lin, T.-K.; Wang, J.-C. Cross-Talk Immunity of PEDOT:PSS Pressure Sensing Arrays with Gold Nanoparticle Incorporation. *Sci. Rep.* **2017**, *7*, 12252.
(21) Pan, L.; Chortos, A.; Yu, G.; Wang, Y.; Isaacson, S.; Allen, R.; Shi, Y.; Dauskardt, R.; Bao, Z. An Ultra-sensitive Resistive Pressure Sensor Based on Hollow-sphere Microstructure Induced Elasticity in Conducting Polymer Film. *Nat. Commun.* **2014**, *5*, 3002.
(22) Siqueira, J. R.; Oliveira, O. N. *Carbon-Based Nanomaterials, Nanostructures*; Elsevier: New York, 2017; Chapter 8, pp 233−249.
(23) Lee, X. J.; Hiew, B. Y. Z.; Lai, K. C.; Lee, L. Y.; Gan, S.; Thangalazhy-Gopakumar, S.; Rigby, S. Review on Graphene and Its Derivatives: Synthesis Methods and Potential Industrial Implementation. *J. Taiwan Inst. Chem. Eng.* **2019**, *98*, 163−180.
(24) Zhang, Y.; Huang, Y.; Chen, H.; Huang, Z.; Yang, Y.; Xiao, P.; Zhou, Y.; Chen, Y. Composition and Structure Control of Ultralight Graphene Foam for High-performance Microwave Absorption. *Carbon* **2016**, *105*, 438−447.
(25) Chen, D.; Feng, H.; Li, J. Graphene Oxide: Preparation, Functionalization, and Electrochemical Applications. *Chem. Rev.* **2012**, *112*, 6027−6053.
(26) Yeh, T.-F.; Teng, C.-Y.; Chen, L.-C.; Chen, S.-J.; Teng, H. Graphene Oxide-based Nanomaterials for Efficient Photoenergy Conversion. *J. Mater. Chem. A* **2016**, *4*, 2014−2048.
(27) Dreyer, D. R.; Park, S.; Bielawski, C. W.; Ruoff, R. S. The Chemistry of Graphene Oxide. *Chem. Soc. Rev.* **2010**, *39*, 228−240.
(28) Niu, J.; Yang, D.; Ren, X.; Yang, Z.; Liu, Y.; Zhu, X.; Zhao, W.; Liu, S. Graphene-Oxide Doped PEDOT:PSS As a Superior Hole Transport Material for High-Efficiency Perovskite Solar Cell. *Org. Electron.* **2017**, *48*, 165−171.
(29) Park, Y.; Soon Choi, K.; Young Kim, S. Graphene Oxide/PEDOT:PSS and Reduced Graphene Oxide/PEDOT:PSS Hole

DOI: 10.1021/acsami.9b10575
ACS Appl. Mater. Interfaces 2019, 11, 34305−34315

Extraction Layers in Organic Photovoltaic Cells. *Phys. Status Solidi A* **2012**, *209*, 1363−1368.
(30) Lee, D.-Y.; Na, S.-I.; Kim, S.-S. Graphene Oxide/PEDOT:PSS Composite Hole Transport Layer for Efficient and Stable Planar Heterojunction Perovskite Solar Cells. *Nanoscale* **2016**, *8*, 1513−1522.
(31) Hasani, A.; Sharifi Dehsari, H.; Asghari Lafmejani, M.; Salehi, A.; Afshar Taromi, F.; Asadi, K.; Kim, S. Y. Ammonia-Sensing Using a Composite of Graphene Oxide and Conducting Polymer. *Phys. Status Solidi RRL* **2018**, *12*, 1800037.
(32) Huang, D.; Li, X.; Wang, S.; He, G.; Jiang, W.; Hu, J.; Wang, Y.; Hu, N.; Zhang, Y.; Yang, Z. Three-Dimensional Chemically Reduced Graphene Oxide Templated by Silica Spheres for Ammonia Sensing. *Sens. Actuators, B* **2017**, *252*, 956−964.
(33) Wu, X.; Liu, J.; Wu, D.; Zhao, Y.; Shi, X.; Wang, J.; Huang, S.; He, G. Highly Conductive and Uniform Graphene Oxide Modified PEDOT:PSS Electrodes for ITO-Free Organic Light Emitting Diodes. *J. Mater. Chem. C* **2014**, *2*, 4044−4050.
(34) Sun, Y.; Tang, J.; Zhang, K.; Yuan, J.; Li, J.; Zhu, D.-M.; Ozawa, K.; Qin, L.-C. Comparison of Reduction Products From Graphite Oxide and Graphene Oxide for Anode Applications in Lithium-Ion Batteries and Sodium-Ion Batteries. *Nanoscale* **2017**, *9*, 2585−2595.
(35) Xu, J.; Tan, Z.; Zeng, W.; Chen, G.; Wu, S.; Zhao, Y.; Ni, K.; Tao, Z.; Ikram, M.; Ji, H.; Zhu, Y. A Hierarchical Carbon Derived from Sponge-Templated Activation of Graphene Oxide for High-Performance Supercapacitor Electrodes. *Adv. Mater.* **2016**, *28*, 5222−5228.
(36) Tanese, M. C.; Farinola, G. M.; Pignataro, B.; Valli, L.; Giotta, L.; Conoci, S.; Lang, P.; Colangiuli, D.; Babudri, F.; Naso, F.; Sabbatini, L.; Zambonin, P. G.; Torsi, L. Poly(alkoxyphenylene−thienylene) Langmuir−Schäfer Thin Films for Advanced Performance Transistors. *Chem. Mater.* **2006**, *18*, 778−784.
(37) Osburn, C. M.; Huff, H. R. *MOSFET Device Scaling: A (Biased) History of Gate Stacks in ECS PV 2002-01*, Abstract No. 366, 2002.
(38) The Scaling of MOSFETs, Moore's Law, and ITRS. Internet: http://userweb.eng.gla.ac.uk/fikru.adamu-lema/Chapter_02.pdf, (accessed April 2, 2019).
(39) Rivnay, J.; Mannsfeld, S. C. B.; Miller, C. E.; Salleo, A.; Toney, M. F. Quantitative Determination of Organic Semiconductor Microstructure from the Molecular to Device Scale. *Chem. Rev.* **2012**, *112*, 5488−5519.
(40) Tulevski, G. S.; Nuckolls, C.; Afzali, A.; Graham, T. O.; Kagan, C. R. Device scaling in sub-100nm pentacene field-effect transistors. *Appl. Phys. Lett.* **2006**, *89*, 183101.
(41) Choi, S.; Potscavage, W. J., Jr.; Kippelen, B. Area-Scaling of Organic Solar Cells. *J. Appl. Phys.* **2009**, *106*, 054507.
(42) FlexiForce A101 Sensor. https://www.tekscan.com/products-solutions/force-sensors/a101, (accessed April 4, 2019).
(43) Wang, J.-C.; Karmakar, R.; Lu, Y.-J.; Huang, C.-Y.; Wei, K.-C. Characterization of Piezoresistive PEDOT:PSS Pressure Sensors with Inter-Digitated and Cross-Point Electrode Structures. *Sensors* **2015**, *15*, 818−831.
(44) Moulder, J. F.; Stickle, W. F.; Sobol, P. E.; Bomben, K. D. *Handbook of X-Ray Photoelectron Spectroscopy*; Perkin-Elmer Corp., Physical Electronics Division: Eden Prairie, MN, 1992.
(45) Spanninga, S. A.; Martin, D. C.; Chen, Z. X-ray Photoelectron Spectroscopy Study of Counterion Incorporation in Poly(3,4-ethylenedioxythiophene) (PEDOT) 2: Polyanion Effect, Toluenesulfonate, and Small Anions. *J. Phys. Chem. C* **2010**, *114*, 14992−14997.
(46) Ganguly, A.; Sharma, S.; Papakonstantinou, P.; Hamilton, J. Probing the Thermal Deoxygenation of Graphene Oxide Using High-Resolution In Situ X-ray-Based Spectroscopies. *J. Phys. Chem. C* **2011**, *115*, 17009−17019.
(47) Briggs, D.; Beamson, G. XPS Studies of the Oxygen 1s and 2s Levels in a Wide Range of Functional Polymers. *Anal. Chem.* **1993**, *65*, 1517−1523.
(48) Petraki, F.; Kennou, S.; Nespurek, S.; Biler, M. A Spectroscopic Study for the Application of a PEDOT-type Material as Buffer Layer in Electronic Devices. *Org. Electron.* **2010**, *11*, 1423−1431.
(49) Tao, C.-a.; Wang, J.; Qin, S.; Lv, Y.; Long, Y.; Zhu, H.; Jiang, Z. Fabrication of pH-sensitive graphene oxide-drug supramolecular hydrogels as controlled release systems. *J. Mater. Chem.* **2012**, *22*, 24856−24861.
(50) Xu, B.; Gopalan, S.-A.; Gopalan, A.-I.; Muthuchamy, N.; Lee, K.-P.; Lee, J.-S.; Jiang, Y.; Lee, S.-W.; Kim, S.-W.; Kim, J.-S.; Jeong, H.-M.; Kwon, J.-B.; Bae, J.-B.; Kang, S.-W. Functional Solid Additive Modified PEDOT:PSS as an Anode Buffer Layer for Enhanced Photovoltaic Performance and Stability in Polymer Solar Cells. *Sci. Rep.* **2017**, *7*, 45079.
(51) Goutham Raj, P.; Sandhya Rani, V.; Kanwat, A.; Jang, J. Enhanced Organic Photovoltaic Properties Via Structural Modifications in PEDOT:PSS Due to Graphene Oxide Doping. *Mater. Res. Bull.* **2016**, *74*, 346−352.
(52) Lindfors, T.; Boeva, Z. A.; Latonen, R.-M. Electrochemical Synthesis of Poly(3,4-ethylenedioxythiophene) in Aqueous Dispersion of High Porosity Reduced Graphene Oxide. *RSC Adv.* **2014**, *4*, 25279−25286.
(53) Singh, V.; Arora, S.; Arora, M.; Sharma, V.; Tandon, R. P. Characterization of Doped PEDOT: PSS and its Influence on the Performance and Degradation of Organic Solar Cells. *Semicond. Sci. Technol.* **2014**, *29*, 045020.
(54) Lim, S. P.; Pandikumar, A.; Li, Y. S.; Huang, N. M.; Lim, H. N. In-situ Electrochemically Deposited Polypyrrole Nanoparticles Incorporated Reduced Graphene Oxide as an Efficient Counter Electrode for Platinum-free Dye-sensitized Solar Cells. *Sci. Rep.* **2014**, *4*, 5305.
(55) Lauer, L. J. Raman spectra of Quasi Elemental carbon. In *Handbook of Raman Spectroscopy: From the Research Laboratory to the Process Line*, 1st ed.; Marcel Dekker Inc.; New York Basel, 2001; pp 863−918.
(56) Fogler, M. M.; Teber, S.; Shklovskii, B. I. Variable-range Hopping in Quasi-one-dimensional Electron Crystals. *Phys. Rev. B: Condens. Matter Mater. Phys.* **2004**, *69*, 035413.
(57) Nardes, A. M.; Kemerink, M.; Janssen, R. A. J.; Bastiaansen, J. A. M.; Kiggen, N. M. M.; Langeveld, B. M. W.; van Breemen, A. J. J. M.; de Kok, M. M. Microscopic Understanding of the Anisotropic Conductivity of PEDOT:PSS Thin Films. *Adv. Mater.* **2007**, *19*, 1196−1200.
(58) Efros, A. L.; Shklovskii, B. I. Coulomb Gap and Low Temperature Conductivity of Disordered Systems. *J. Phys. C: Solid State Phys.* **1975**, *8*, L49.
(59) Bai, Y.; Wu, H.; Wu, R.; Zhang, Y.; Deng, N.; Yu, Z.; Qian, H. Study of Multi-Level Characteristics for 3D Vertical Resistive Switching Memory. *Sci. Rep.* **2014**, *4*, 5780.
(60) Entin-Wohlman, O.; Gefen, Y.; Shapira, Y. Variable-Range Hopping Conductivity in Granular Materials. *J. Phys. C: Solid State Phys.* **1983**, *16*, 1161.
(61) van der Pauw, L. J. A Method of Measuring Specific Resistivity and Hall Effect of Disks of Arbitrary Shape. *Philips Res. Rep.* **1958**, *13*, 1.
(62) Ozaki, S.; Wada, Y.; Noda, K. DC Hall-Effect Measurement for Inkjet-Deposited Films of Poly(3,4-ethylenedioxythiophene)/Poly(4-styrenesulfonate) by Using Microscale Gap Electrodes. *Synth. Met.* **2016**, *215*, 28−34.
(63) Ellmer, K. Hall Effect and Conductivity Measurements in Semiconductor Crystals and Thin Films. In *Characterization of Materials*; Kaufmann, E. N., Ed.; John Wiley & Sons, Inc: New Jersey, 2012; pp 564−579.
(64) Noda, K.; Sugawara, A.; Watahiki, T.; Okamoto, K.; Kiyosu, T.; Matsushige, K.; Wada, Y. Hall-Effect Measurement of Organic Semiconductor Layers Using Micro-Scale Electrode Chips. *IEEJ Trans. Electron. Inf. Syst.* **2012**, *132*, 1398−1401.
(65) Van Zeghbroeck, B. *Bipolar Junction Transistors*; University of Colorado: USA, 2011; Chapter 5.
(66) Yeh, E. C. C.; Tu, K. N. Numerical Simulation of Current Crowding Phenomena and Their Effects on Electromigration in Very Large Scale Integration Interconnects. *J. Appl. Phys.* **2000**, *88*, 5680.

DOI: 10.1021/acsami.9b10575
ACS Appl. Mater. Interfaces 2019, 11, 34305−34315

(67) Zhang, P.; Lau, Y. Y.; Gilgenbach, R. M. Analysis of Current Crowding in Thin Film Contacts From Exact Field Solution. *J. Phys. D: Appl. Phys.* **2015**, *48*, 475501.

DOI: 10.1021/acsami.9b10575
ACS Appl. Mater. Interfaces 2019, 11, 34305−34315